CO8-1 Neutron Phase Imaging with Talbot-Lau Interferometer at CN-3

Y. Seki[1], T. Shinohara[1], Y. Matsumoto[2], M. Hino[3], T. Oda[3]

[1]*J-PARC Center, JAEA*
[2]*Comprehensive Research Organization for Science and Society*
[3]*Institute for Integrated Radiation and Nuclear Science, Kyoto University*

INTRODUCTION: Neutron phase imaging using the Talbot-Lau interferometer is a method which causes neutron intensity contrast through the phase shift of the neutron wave and produces a visibility image reflecting smaller structures than spatial resolution of imaging system, which are normally detected by USANS method. Therefore, neutron phase imaging is recognized as a special technique not only giving neutron imaging a good sensitivity to a thin or weak neutron-absorbing object but also connecting real space observation and reciprocal space measurements.
We have been developing this imaging technique using pulsed neutrons at "RADEN" in J-PARC MLF [1, 2], and we have started experiments at CN-3 beam port in Kyoto University Reactor (KUR) from 2018, so as to confirm the feasibility applying neutron phase imaging to small/medium flux neutron source facilities. In the previous study, we have succeeded to obtain moire images at the CN-3 beam port by using a portable Talbot-Lau interferometry system, but the exposure time was very long and the resulting visibility was not high enough. In this work, we have prepared a new set of gratings optimized to the neutron spectra of the CN-3 port and introduced a new detector system using a sCMOS camera.

EXPERIMENTS: The Talbot-Lau interferometer consists of three gratings (G0, G1, and G2), and the design parameter of these gratings roughly depends on the central wavelength, where visibility becomes maximum, and the distances between gratings. The previous gratings are designed to suit the central wavelength of 5 Å to get good sensitivity against the phase shift, but this design parameter didn't make use of the neutron spectrum at CN-3 beam port. Hence, we have prepared a set of new gratings which is optimized to the CN-3 beam port having the central neutron wavelength of 2.7 Å. In addition, the size of grating was increased to 6 cm x 6 cm to increase the Field of View. The imaging detector was replaced to a system composed of a sCMOS camera (ORCA-Flash4.0 V3, Hamamatsu Corporation) and a ^{6}LiF/ZnS(Cu) scintillator with the thickness of 200 μm.
The phase imaging experiment was performed by means of "phase-stepping method" in which the G2 grating travels horizontally for a period of the grating with several steps more than 5. Then the intensity profile against the step number was analyzed at each position to produce three images: differential phase image, visibility image and absorption image.

RESULTS: At first, we have studied the performance of the new gratings. A moire image was obtained in an exposure time of only 10 sec, while more than 1 min was needed using the previous setup (Fig.1 left). The evaluated visibility was around 42%, which was two times higher than previous one, without severe inhomogeneity (Fig.1 right).

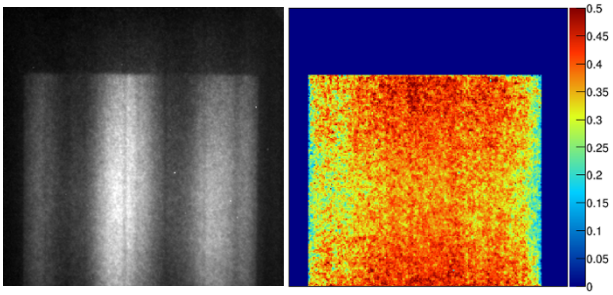

Fig. 1. Moire image obtained with new gratings and detector system (right) and evaluated visibility image by phase-stepping method (left).

Then, we have conducted visibility imaging experiments using this imaging system. Additively manufactured Inconel rods (10mm-ϕ and 70 mm-L), where one was as-made and the other was annealed, were used as samples. The exposure time for each step was 100 sec and the step number was 8. The obtained visibility images shown in Fig. 2 indicates different contrast between two samples. This result suggests that the micro structure of as-made sample was disappeared due to annealing, this means that the grain structure constructed by additive manufacturing process was homogenized by annealing. Thus, the neutron phase imaging can be applied to study inhomogeneity of microstructures in a metallic object.

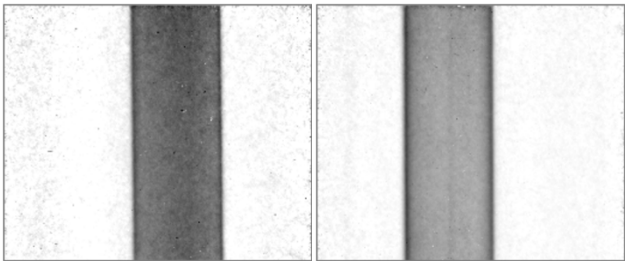

Fig. 2. Visibility images for Inconel sample. Right image is for as-made and left one is for annealed sample.

ACKNOWLEDGEMENT: This work was supported by JST ERATO Momose Quantum Beam Phase Imaging Project, Grant Number JPMJER1403. We would like to thank Dr. T. Samoto of Tohoku University for the fabrication of gratings used in this study.

REFERENCES:
[1] T. Shinohara *et al.*, Rev. Sci. Instr, **91** (2020) 012007.
[2] Y. Seki *et al.*, EPL, **123** (2018) 12002.

CO8-2 Study on the Visualization of Organic Matter between Metals to Contribute to the Advancement of the Industrial Products

K. Hirota, H. M. Shimizu[1], M. Kitaguchi[1], Y. Tsuchikawa[1], N. Yamamoto[1], A. Uritani[2], K. Watanabe[2], S. Yoshihashi[2], A. Yamazaki[2], D. Ito[3] and Y. Saito[3]

RCNP, Osaka University
[1]Graduate School of Science, Nagoya University
[2]Graduate School of Engineering, Nagoya University
[3]Institute for Integrated Radiation and Nuclear Science, Kyoto University

INTRODUCTION: Mechanical and industrial products such as automobiles and aircraft are progressing with higher performance and higher accuracy in Japan. One of the demands at the development site of these state-of-the-art products is a visualization of the state of organic materials (oil film, grease, electrolyte, etc.) existing between metals, which can not be seen directly by our eyes. In this research, we will explore the possibility of observing the dynamic state of the organic materials (shape, properties, thickness distribution) and its dynamic change mainly between automobile parts as an example.

At present Nagoya University is constructing an accelerator-driven small neutron source (NUANS) and neutron radiography ports [1]. We are planning an in-site measurement of the fuel cell during power generation. And we are also proceeding with the quantitative evaluation of the CCD output image. This year, we produced a neutron camera for radiography to be used at NUANS, so we evaluated its performance in KUR E2 port.

EXPERIMENTS: In fuel cell development, the elimination of water from the electrode during power generation is a very important issue. In order to visualize the movement of minute water in the transmission image, we constructed a new evaluation software. Images were acquired for the evaluation of the constructed software. A groove with a width of 1 mm is made on an aluminum plate, and neutrons are irradiated in the state of accumulating water to acquire the image. Next, the movement of the water was simulated by moving this plate. The results obtained are shown in Fig. 1. In this figure, the aluminum plate is moving upward at 10 mm/s. The water image can be seen only at the first and last places, and is almost invisible while moving. When the moving speed is set to 2 mm / s, the water images appear to be continuous. In this way, we can understand the relationship between water movement and visualization.

FOCUS ADJUSTMENT: Focusing work is very important to visualize a fine image, but in neutron transmission image measurement, this work usually confirms the focus position by taking multiple images and comparing them by human eyes. The focus position is depending on the person who works and the measurement conditions. To obtain the same result irrespective of the person who performed it, it was decided to evaluate the focus adjustment quantitatively. For focus adjustment, it is necessary to perform edge extraction on the acquired image. The image obtained by the CCD camera is subjected to a noise filter for removing the CCD element error and an FFT (Fast Fourier transform) filter for removing the neutron intensity distribution dependency, and then the second derivative of the space (Laplace calculation). Since the Laplacian filter is easily affected by noise, it is necessary to eliminate noise such as dot filtering using a noise filter. Focus adjustment by this edge extraction method was able to determine the focus position correctly. In addition, the neutron irradiation time required for this work is two digits shorter or more than that when it is identified by human eyes. It may be possible to build an autofocus function in the future.

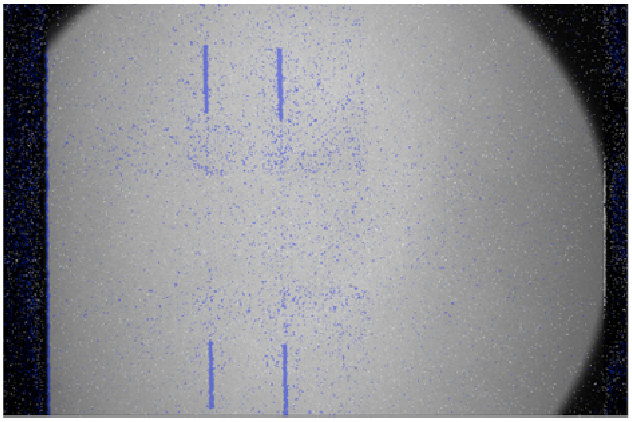

Fig. 1. Measurement of the water motion.

REFERENCES:

[1] K.Hirota, *et al*., EPJ Web of Conf. **231**(2020)05002.

CO8-3 Measurements of multiphase flow dynamics using neutron radiography

Y. Saito and D. Ito

Institute for Integrated Radiation and Nuclear Science, Kyoto University

INTRODUCTION: Neutron radiography (NRG) is a powerful tool for multiphase flow visualization as well as ordinary fluid dynamics. As one of the applications of NRG, gas-liquid two-phase flows in a metallic pipe have been clearly visualized by using NRG. However, the measurement accuracy of thin liquid film formed in such two-phase flows has not been fully evaluated. The liquid film thickness is one of the important parameters to investigate the two-phase flow behavior. In this work, our neutron imaging system has been modified to realize more sophisticated flow visualization and precise measurements of thin liquid film.

DEVELOPMENT OF HIGH-SPEED NEUTRON IMAGING SYSTEM: A high-speed neutron imaging system for flow visualization has been developed at the B-4 supermirror neutron guide facility [1] of the Institute for Integrated Radiation and Nuclear Science, Kyoto University. This imaging system consists of a neutron converter, a dark box with a single mirror, an ultrasensitive lens, an optical image intensifier and a high-speed camera. The high frame rate up to 10,000 frame/sec could be achieved using above-mentioned combination at the B-4 port [2]. The pixel resolution and frame rate can be adjusted by selecting the optics.

VISUALIZATION OF SIMULATED THIN FILM: Neutron imaging experiments were conducted at the E-2 port of the Kyoto University Research Reactor. In this port, the neutron flux is 1×10^5 n/cm^{2}s, and the beam size is 15 cm in diameter. CCD camera system was employed, and the static film thickness was estimated from the neutron transmission images. As a preliminary work, the liquid film formed in two-phase flows was simulated by the thin polyimide sheet and the thickness was varied from 75 μm to 250 μm. The polyimide has the macroscopic neutron cross-section of 1.3cm^{-1}. The film sample and rotation stage are shown in Fig.1. The angle of the polyimide film was set at 0~75 degrees. The neutron transmission images of the polyimide film with the thickness of 250 μm are shown in Fig.2. At smaller angle conditions, there is little change in the transmission. However, at the angle of 75 degrees, the neutron attenuation changes obviously. The mean value of the neutron transmission in the polyimide film area is plotted in Fig.3, and they are compared with the results of geometric calculation. Most of the results show good agreement, however, some measured results with the transmission values larger than 0.98 depart from the calculation results. It would be suggested that the estimation of very thin film should be a challenging problem in present neutron imaging technique. In the next step, the measurement error in the film thickness shall be quantitively estimated by improving the imaging system and processing method.

Fig. 1 Sample and rotation stage.

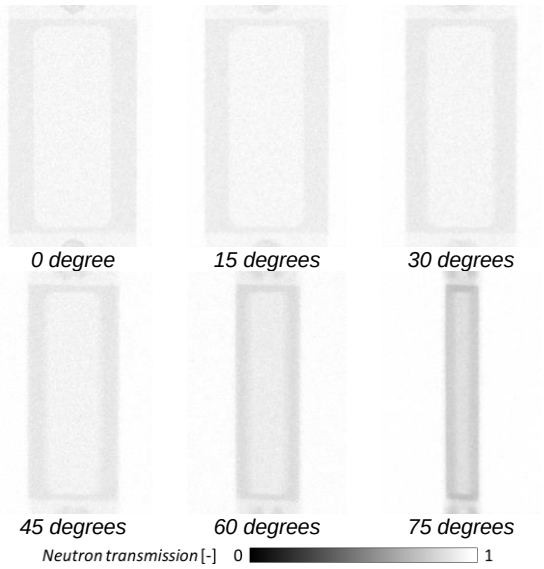

Fig. 2 Neutron transmission images of polyimide sheet (δ = 250 μm).

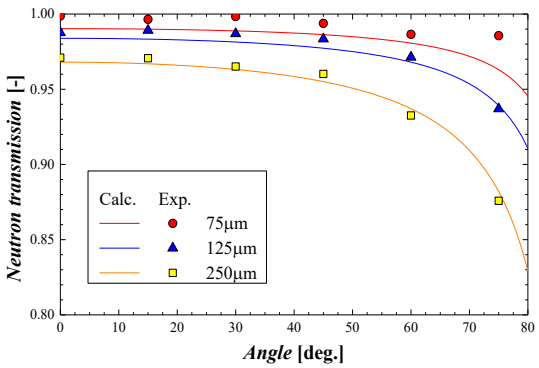

Fig. 3 Angle dependence of neutron transmission.

REFERENCES:

[1] Y. Saito, *et al*., Nucl. Instr. Meth. Phys. Res., A, **651** (2011) 36-41.

CO8-4 Visualization of Hydrogen in Pure Palladium via Neutron Radiography and Tomography

K. Shimizu[1], H. Toda[2], K. Hirayama[2], H. Fujihara[2], D. Ito[3], Y. Saito[3]

[1]*Department of Physical Science and Materials Engineering, Iwate University*
[2]*Department of Mechanical Engineering, Faculty of Engineering, Kyushu university*
[3]*Institute for Integrated Radiation and Nuclear Science, Kyoto University*

INTRODUCTION: It is widely recognized that hydrogen in metallic materials degrades the mechanical properties of the materials. Various hydrogen embrittlement mechanisms, such as HELP, HEDE and HESIV have been proposed to date [1], but there is still no comprehensive interpretation. However, for each mechanism, it is consistent that hydrogen trapping and the resulting localization of hydrogen to defects and microstructures are the dominant factors of hydrogen embrittlement [2]. To understand the hydrogen embrittlement, it is necessary to visualize the hydrogen distribution and to elucidate its evolutionary behavior over time. In this study, hydrogen in a metal was visualized by neutron radiography and tomography, and hydrogen accumulation under stress was assessed. Several palladium specimens with different hydrogen contents were prepared and a notch was introduced. It has been demonstrated that hydrogen content can be analyzed by neutron tomography, and the possibility of evaluating hydrogen accumulation under stress is discussed.

EXPERIMENTS: Palladium specimens with hydrogen contents of 0 at%, 10 at%, and 20 at% were prepared for neutron imaging. Hydrogen content was controlled by high temperature hydrogen exposure. Neutron radiography was performed on the KUR E-2 port [3]. The imaging system consists of a ^{6}LiF:ZnS visible light converter and a cooled CCD detector. The exposure time was set to 5 min at a thermal power of 1 MW in the research reactor. Neutron tomography was also performed at the KUR E-2 port. A rotating stage for tomographic observation was added to that of radiography. Neutron transmission images were obtained by rotating the specimen from 0 to 180° in 1° increments. Total 180 images were reconstructed in a 3D image using a convolutional back projection algorithm.

RESULTS: Fig. 1 shows tomographic cross-sectional images of the central part of specimens before and after tensile loading. Fig. 1(d) shows the profile of CT value obtained from the white lines in Fig. 1(a-c). The contrast between 0%H and 10%H at no load indicates that the difference in hydrogen content can be evaluated from image contrast as well as the transmission image. On the other hand, no hydrogen accumulation was observed when comparing before and after tensile loading at 10% H. The location of x = 3 mm in Fig. 1(d) corresponds to the notch tip of specimen, but the change in hydrogen content before and after loading could not be measured even in the line profile. This was true not only at the center of specimens shown in Fig. 1(a-c), but also near the surface. The notch opening displacement was measured to be about 510 μm. The plastic zone size of the notch tip was calculated to be about 220 μm by estimating the applied stress of the specimen from the opening displacement. It is inferred that the hydrogen accumulation is remarkable in this region. The measured tomographic image has a resolution of about 400 μm. This suggest that hydrogen accumulation was not visualized in Fig. 1(c) and (d), because of accumulation region was smaller than 400 μm. It is expected that short-time 3D imaging with a spatial resolution of 200 μm is available by upgrading the imaging system. Using this system, 3D/4D analysis of hydrogen accumulation behavior will be revealed by neutron tomographic observation.

REFERENCES:

[1] I. M. Robertson *et al.*, Metall. Mater. Trans. A 46 (2015) 1085-1103..
[2] Z. Zhang *et al.*, Acta. Mater. 113 (2016) 272–283.
[3] Y. Saito *et al.*, J. Jpn. Soc. Precis. Eng. 79 (2013) 822–825.
[4] K. Shimizu *et al.*, J. Japan Inst. Met. Mater. 83 (2019) 434–440.

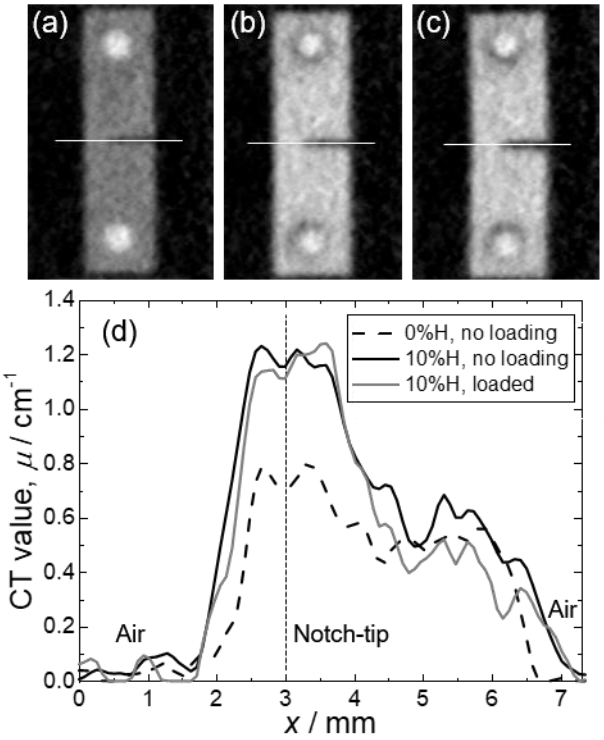

Fig. 1. Virtual cross-sections of the 3D neutron tomographic images; (a) palladium without hydrogen, (b) that with 10 % hydrogen, and (c) that with 10 % hydrogen after loading. (a) and (b) were observed without loading. (d) Line profiles obtained from the white solid lines in (a~c).

CO8-5

Visualization and Measurement of Boiling Flow Behaviors in Parallel Mini-channel Heat Exchanger

H. Asano, H. Murakawa, R. Moriyasu, S. Inoue, K. Sugimoto, D. Ito[1] and Y. Saito[1]

Department of Mechanical Engineering, Kobe University
[1] Institute for Integrated Radiation and Nuclear Science, Kyoto University

INTRODUCTION: Microchannel compact heat exchangers are paid attention for the compactness and reduction in temperature difference between fluids. Since smaller diameter leads to larger pressure loss, micro channel heat exchanger has many parallel channels. Therefore, in the case that the heat exchanger is used for evaporator, refrigerant flow distribution often causes a deterioration in the heat transfer performance. In this study, boiling flow behaviors in a single layer microchannel heat exchanger had been visualized by neutron radiography, and void fraction distributions had been measured from the radiographs.

EXPERIMENTS: The tested heat exchanger was manufactured by diffusion bonding of thin stainless steel plates, and consists of single-layer refrigerant and heating medium parallel channels. The channel cross-section and flow arrangement are shown in Fig. 1 and 2, respectively. HFC-134a and FC3283 were used as the refrigerant and the heating medium, respectively. The number of channels are 21 for the refrigerant and 20 for the heating medium. Each channel has semicircular cross-section. The heat exchanger was placed in vertical plane to form vertically upward boiling flows of the refrigerant. To avoid maldistribution of refrigerant flows, two kinds of divided ribs, such as perforated and offset types, as shown in Fig. 3 are used. Radiographs were recorded by a cooled CCD camera with the exposure time of 30 seconds and the pixel size of 88 μm/pixel.

RESULTS: Void fraction was measured for each pixel of visualized images, and the distributions for the test sections with the straight parallel channels, the perforated and offset type channels of refrigerant are shown in Fig. 4 (a) to (c), respectively. It can be clearly observed that the void fraction on the right side close to the heating medium inlet was higher than the left side due to the larger temperature difference. It was seemed that void fraction distribution became more homogeneous for the perforate rib. In this case, the inlet condition of refrigerant was a subcooled liquid. The onset of boiling might affect the flow distribution. For the perforated type, the holes through the ribs might help bubble nucleation and development of two-phase flows.

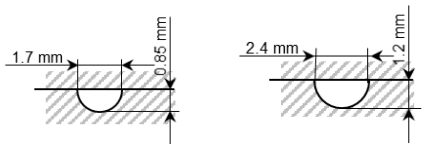

(a) R134a (b) FC3283

Fig.1. Channel cross-section.

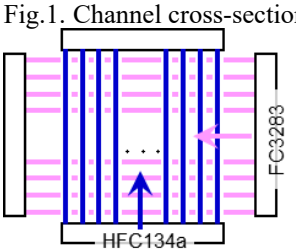

Fig. 2. Flow arrangement.

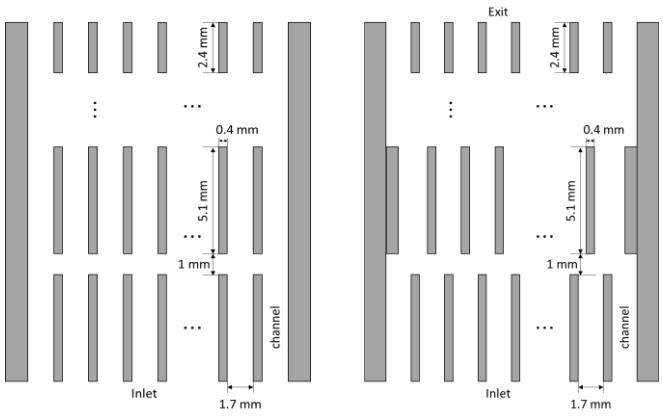

(a) Perforated type (b) Offset type

Fig. 3. Rib pattern in refrigerant channel.

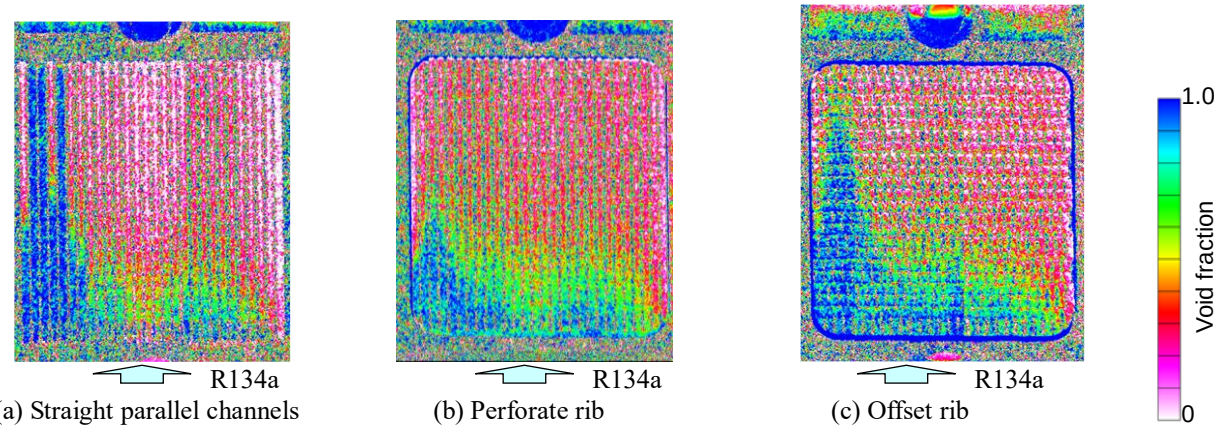

(a) Straight parallel channels (b) Perforate rib (c) Offset rib

Fig. 4. Void fraction distributions (mass flux : 150 kg/(m^2・s) for R134a, 920 kg/(m^2・s) for FC3283, inlet temperature : 50 ℃ for FC3283) .

CO8-6 Evaluation of Water Distribution and Electrochemical Characteristics in Polymer Electrolyte Fuel Cell

H. Murakawa, S. Torii, K. Mine, K. Sugimoto, H. Asano, D. Ito[1] and Y. Saito[1]

Graduate School of Engineering, Kobe University

[1]Institute for Integrated Radiation and Nuclear Science, Kyoto University

INTRODUCTION: Water management is a key topic of a polymer electrolyte fuel cell (PEFC). If condensed water exists in the gas diffusion layer (GDL) and the gas channel, it may depress the gas diffusion as flooding. Furthermore, loss in electric power generation in PEFCs is due to resistances such as ionic, activation, concentration, etc. Many of these resistances are related to the mass transport in the PEFC. To evaluate the resistances in a PEFC, electrochemical impedance spectroscopy (EIS) has been widely used [1]. However, the effect of water in the PEFC on the resistances has not been fully understood. Aim of this study is to clarify the effect of water in the PEFC on the resistances. Simultaneous measurements of the water distribution and the electrical impedance were carried out by using neutron radiography and EIS. Changes in water accumulation in the PEM and the GDL were compared with the resistances.

EXPERIMENTS: A small size PEFC having a single-serpentine gas-channel with cross-sectional area of 1 × 1 mm^2 was used for measuring two-dimensional water distribution and the electrochemical characteristics. Nafion® NR-212 was used as the PEM with a thickness of approximately 90 μm having catalyst layers on both the anode and cathode sides. The GDL was carbon paper (Toray Ind.) with thickness of 190 μm at the cathode side and 280 μm at the anode side. The porosity of the GDL was approximately 78%. Two-dimensional water distributions were obtained every 60 sec during the PEFC operation. The EIS measurements were simultaneously carried out with the neutron radiography for evaluating the PEM resistance and the reaction resistance, R_{CT} [Ω]. The hydrogen and air flow rates were 84 and 196 cc/min, respectively. The experiments were carried out at room temperature, while the temperature of the PEFC varied between 25 – 30 °C.

RESULTS: Two-dimensional water distributions at current density i =316 and 500 mA/cm^2 are compared in Fig. 1. Measurement area is between 4th and 6th channels, and the top channel in the figure is the upstream position. Liquid water accumulation during the PEFC operation can be confirmed as indicated by the gray-scale. The time represents the elapse time from the power generation. Amounts of water accumulation in the GDL under the lands and channels are different and a large amount of water existed under lands at the earlier results. It indicated that water accumulation is started under the lands. Then, liquid water reaches channel and are particularly concentrated on the land corners. Difference of the water distributions at 9 and 15 min is not significant for i = 316 mA/cm^2. Therefore, it can be confirmed that the water distributions are almost steady states after 9 min. On the other hand, water gradually accumulated in the channel for i =500 mA/cm^2. The water accumulation at downstream channel, *i.e.* 6th channel, is greater than that at 4th channel. This is because the relative humidity becomes higher at downstream position, and the water accumulation is easy to occur.

Fig. 2 represents change of the reaction resistance, R_{CT}. R_{CT} gradually decreases until 15 min at i = 316 mA/cm^2. For i = 400 mA/cm^2, R_{CT} gradually decreases until 9 min, and it became almost constant after the time. Furthermore, it gradually increases after 2 min for i = 500 mA/cm^2. As confirmed from the water distribution, the much water accumulation was confirmed in the channel. This prevent the water supply to the GDL resulting in increases of the concentration resistance. However, the effect was not significant although water accumulation was clearly confirmed in the channels at 15 min for i = 500 mA/cm^2.

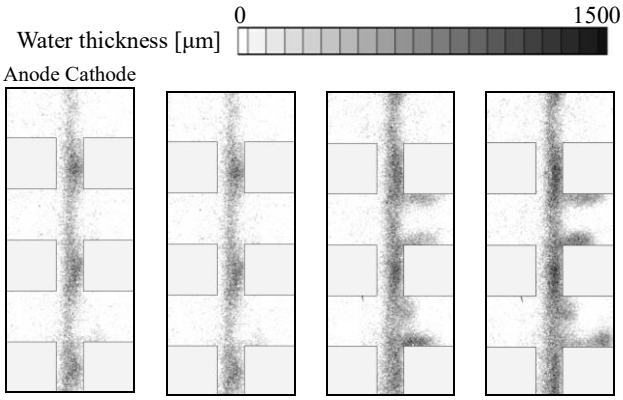

(a) i = 316 mA/cm^2 (b) i = 500 mA/cm^2

Fig. 1. Two-dimensional water distributions.

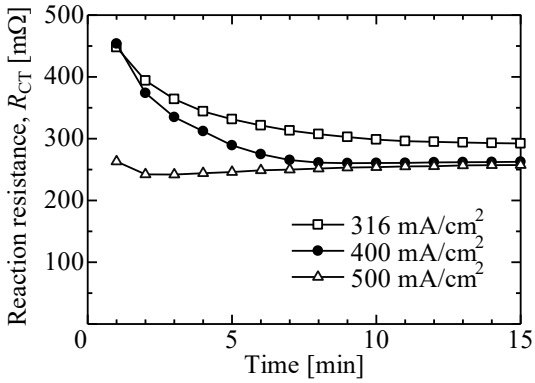

Fig. 2. Time-series of the reaction resistances.

REFERENCES:

[1] E. Antolini, *et al.*, J. Power Sources, **77** (1999) 136-142.

CO8-7 Meltwater Behavior During the Defrosting Process by using Neutron Radiography

R. Matsumoto, T. Shiokawa[1], Y. Nishiura[1], T. Makihara[1], D. Ito[2] and Y. Saito[2]

Faculty of Engineering Science, Kansai University
[1]Graduate School of Science and Engineering, Kansai University
[2]Institute for Integrated Radiation and Nuclear Science, Kyoto University

INTRODUCTION: The frost formation on heat exchanger causes serious problem to the heat transfer performance by thermal resistance between the cold surface and the humid ambient air. Defrosting is important to keep the heat transfer performance of the heat exchanger. The defrosting operations were carried out periodically by the reverse cycle on the air conditioning systems, or the electrical heating on the domestic refrigerators. The frost layer has a micro porous structure with ice crystals and air pores. The meltwater penetrates into the remaining frost layer by the capillary effect through the micro porous. In this study, the meltwater behavior on the aluminum plate-fin-tube heat exchanger was measured by using neutron radiography. The water deposition distribution on the heat exchanger was estimated quantitatively by neutron beam attenuation during the defrosting period.

EXPERIMENTS: Fig.1 shows the schematic view of the experimental apparatus. Cooled humid air adjusted to the flow rate 70 L/min was supplied to the test section. The test section consisted of styrofoam block duct with a cross section of 68 mm x 25 mm and the aluminum plate fin-tube heat exchanger. The heat exchanger consisted by 6 fins with 60 mm in height, 28 mm in width, 0.25 mm in thickness, and together with two tubes of an outer 8.5 mm. Fig.2 shows the aluminum heat exchanger used in this experiment. Fin pitch was 5 mm. On the frosting process, the heat exchanger was cooled by circulating the -25 ºC fluorinert for 66 min. After the frost formation, the air flow was stopped, and the coolant flow was switched to 1°C coolant for defrosting. The water deposition on the heat exchanger was observed by CCD camera (Princeton Inst., 16-bit, 1024×1024 pixels) with image intensifier (Toshiba Electron Tubes & Dev., E5830NE-P4K). Exposure time is 0.15sec. The procedure of the image processing is referred to ref.[1].

RESULTS: Fig.3 shows the water deposition on the heat exchanger during the defrosting process. The main flow direction is right to left in Fig.3. Fig.3(a) shows the frost formation just before the defrosting. Frost was formed almost uniformly on the fin surface except the wake area of the tubes. In Fig.3(b) at 1min53sec from starting the defrost, frost near the tubes are melted and the meltwater penetrated into the remaining frost layer. In Fig.3(c) at 3min2sec, the frost melting spreads around the tubes, and the meltwater is hold in the remaining frost layer at the leading edge of fins. In Figs.3(d) and (e), meltwater flows down to the bottom of the heat exchanger due to the water saturation in frost layer. Finally, the meltwater is discharged from the bottom of the fin, and no melted water remains on the fin surface. This results suggested the smooth removal of the meltwater by the water penetration into the remaining frost layer.

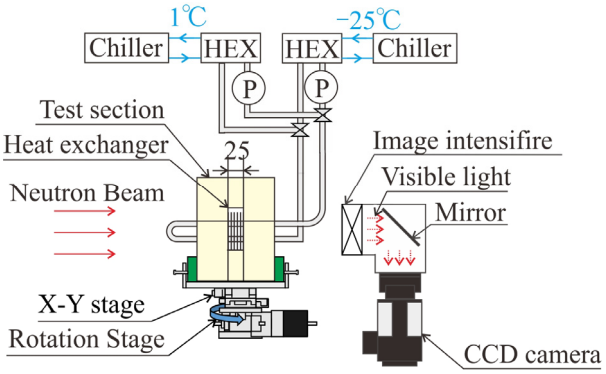

Fig.1. Schematic view of the experimental apparatus.

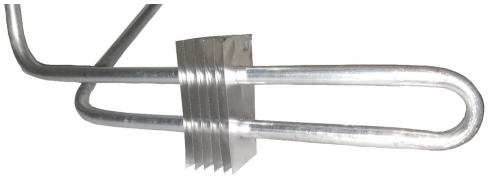

Fig. 2. Plate-fin tube heat exchanger.

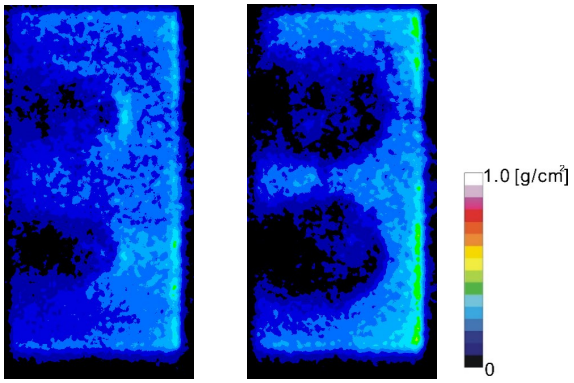

(a) 0 min (b) 1 min 53sec

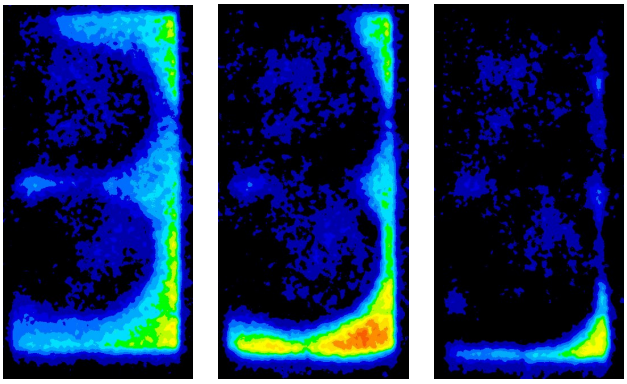

(c) 3min2sec (d) 4min58sec (e) 7min39sec

Fig.3. Meltwater behavior in defrosting process.

REFERENCE:

[1] R. Matsumoto, *et al.,* Proceedings of the International Heat Transfer Conference IHTC-15, IHTC15-9144, Kyoto, pp. 3603-3615.

CO8-8 Flow visualization of heavy oil in supercritical water using neutron radiography

T. Tsukada, M. Kubo, E. Shoji, N. Ito, T. Kaneko, S. Kodaira, S. Takami[1], K. Sugimoto[2], D. Ito[3], Y. Saito[3]

Dept. of Chemical Engineering, Tohoku University
[1] Dept. of Materials Science and Engineering, Nagoya University
[2] Dept. of Mechanical Engineering, Kobe University
[3] Institute for Integrated Radiation and Nuclear Science, Kyoto University

INTRODUCTION: With an increase in the demand for petrochemical feedstock and middle distillate, utilization of heavy oil such as atmospheric or vacuum residue is also necessary. Since the heavy oil has high viscosity and its quality is low, desulfurization and upgrading processes are required to use the heavy oil effectively. In such a situation, upgrading process using supercritical water has been proposed and studied recently.

Understanding of flow behavior of heavy oil in reactors filled with supercritical water is important to improve the performance of upgrading process. However, the phenomena are too complicated to simulate numerically. Since, in experiment, the reactor is made of metal for operation at high pressure and high temperature, the visualization using visible light is not available. Thus, the numerical simulation and experimental flow visualization of heavy oil flow in supercritical water have not been conducted. In our previous study [1], we have visualized the heavy oil flow in a trickle bed reactor under N_2 atmosphere using neutron radiography, and indicated the potential of neutron radiography to investigate the flow behavior of heavy oil. Therefore, as a next step, the visualization of the heavy oil behavior in supercritical water by neutron radiography was carried out, continuing from last year.

EXPERIMENTS: In neutron radiography for the flow visualization of heavy oil in supercritical water, the Kyoto University Research Reactor (KUR) was utilized as neutron source. A series of neutron radiography experiments was conducted with a thermal neutron flux of 8.5×10^7 n/(cm^2·s).

The reactor consists of a 1/2-inch stainless steel tube filled with Al_2O_3 particles with a diameter of 3 mm. The heavy oil, i.e., atmospheric residue (AR), was supplied to a reactor from above with the flow rates of 2.5 or 5.0 g/min. On the other hand, the water was supplied counter-currently with the flow rates ranged from 0.05 to 7.5 g/min. The reactor was heated to temperatures of 400°C and was operated at 25 MPa.

An image intensifier and a camera at the framerate of 30 fps were used to obtain radiography images of the unsteady flow behavior. An image processing to reduce noises and to calculate neutron attenuation was performed for the obtained radiography images.

RESULTS: The flow behavior of heavy oil in the reactor varied depending on the experimental conditions were visualized using neutron radiography. Fig. 1 shows the time variation of flow behavior of heavy oil in supercritical water at the flow rates of heavy oil (ω_o) and water (ω_w) were 2.5 g/min and 0.05 g/min, respectively.

Fig. 2 shows the variations in the area-averaged neutron attenuation ($\overline{\mu\rho d}$) over time, which were calculated over the 8 mm (40 pixels) × 40 mm (200 pixels) area shown in the inset of Fig. 2 under the four experimental conditions. The area-averaged neutron attenuation increased with time and reached a constant value under all the tested conditions. The time required to reach a constant attenuation became longer with increasing supercritical water flow rate, particularly at ω_o = 2.5 g/min. In addition, Case D shows the increase in the attenuation after 40 s due to the upward flow of heavy components of oil from the bottom of the reactor.

CONCLUSION: The results obtained by neutron radiography showed that the flow behavior of heavy oil in the packed bed reactor under supercritical water environment depends on the flow rates of heavy oil and supercritical water.

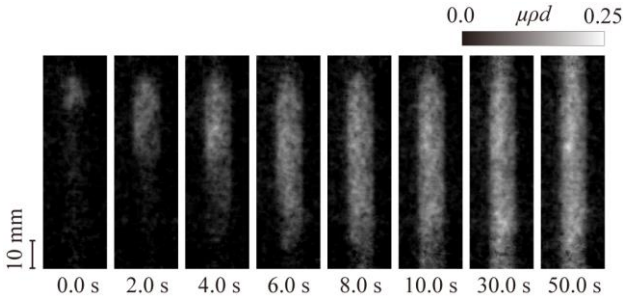

Fig. 1: Flow behavior of heavy oil in supercritical water when the flow rates of heavy oil and water were 2.5 g/min and 0.05 g/min, respectively. μ, ρ, and d are mass attenuation coefficient of thermal neutrons [m^2/kg], density of heavy oil [kg/m^3], and thickness along the neutron beam direction [m].

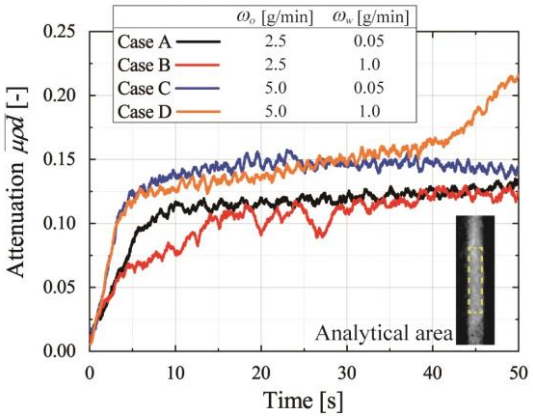

Fig. 2: Time variations of area-averaged neutron attenuation.

REFERENCES:

[1] E. Shoji *et al.*, Chem. Eng. Sci., **196** (2019) 425-432.

CO8-9 Analysis of moisture transfer in high-strength concrete embedded rebar exposed to fire

M. Kanematsu[1], Y. Nishio[1], A. Miyabe[1], K. Kobayashi[1], K. Ueno[1], D. Ito[2], Y. Saito[2], T. Noguchi [3] and M. Tamura[3]

[1]*Department of Architecture, Tokyo University of Science*
[2] *Institute for Integrated Radiation and Nuclear Science, Kyoto University*
[3] *Department of Architecture, The University of Tokyo*

INTRODUCTION: RC structure is fireproof structure, but explosion phenomenon, so called spalling, might occur when subjected to fire especially at high-strength concrete. Thermal stress and water vapor pressure in concrete seems to be the main causes of spalling, therefore, to capture detailed moisture movement in concrete under fire is important to clarify the mechanism of spalling [1]. However, the detailed mechanism of spalling has not been fully understood. In this research, focusing on concrete made of different type of aggregate and on with or without embedded reinforcing bar, we applied neutron radiography (NR) to verify moisture transfer in concrete exposed to fire in order to understand the spalling phenomenon of high strength concrete. We also tried to obtain X-ray transmission images simultaneously.

EXPERIMENTS: Concrete specimens (70×100×30 mm^3) with W / B of 18% were prepared. In some of them, a single rebar (D10, 120mm) with a thermocouple was embedded at 20mm from the bottom surface (Fig.1). The initial relative water content of concrete was about 90%. Graywacke from Ome or limestone from Sano was used for each sample as coarse aggregate. In this experiment, the specimens were heated at the bottom surface with a Bunsen burner. Temperatures in specimen were measured by thermocouples installed in the holes at the position of 10 and 20 mm from the heating surface or attached with rebar. NR was performed at TNRF in the B-4 port of KUR. The angle of view of CCD camera was 100 × 100 mm, and the spatial resolution was about 0.1 mm / pixel.

RESULTS: As shown in Fig. 2, 2 dimensional moisture movement in concrete can be successfully observed. This result shows that embedded rebar can suppress dryness at the backside of concrete, and be apt to condense water and form moisture clog near the heating surface. Comparing the difference in aggregate as shown in Fig.3, concrete of graywacke was apt to condense moisture amount at 10mm depth from the heating surface. However, the time spalling occurred didn't match the time when moisture condensation observed, therefore, further study is needed to clarify the relationship between spalling and moisture movement in concrete.

REFERENCES:

[1] JCI, (2017). "Committee Reports:JCI-TC-154A"

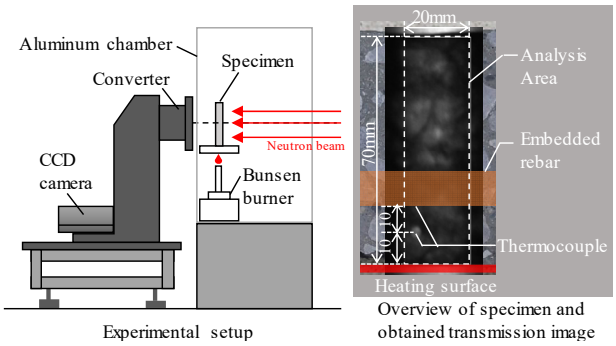

Fig. 1. Outline of Experiment

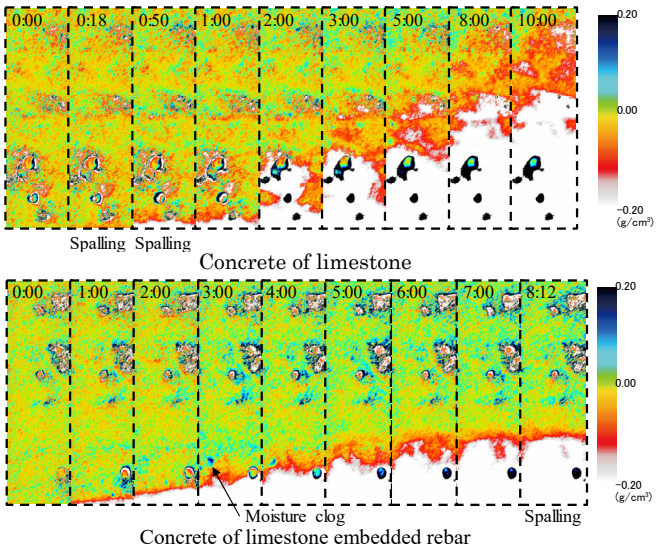

Fig. 2. Relationship between moisture distribution and heating time

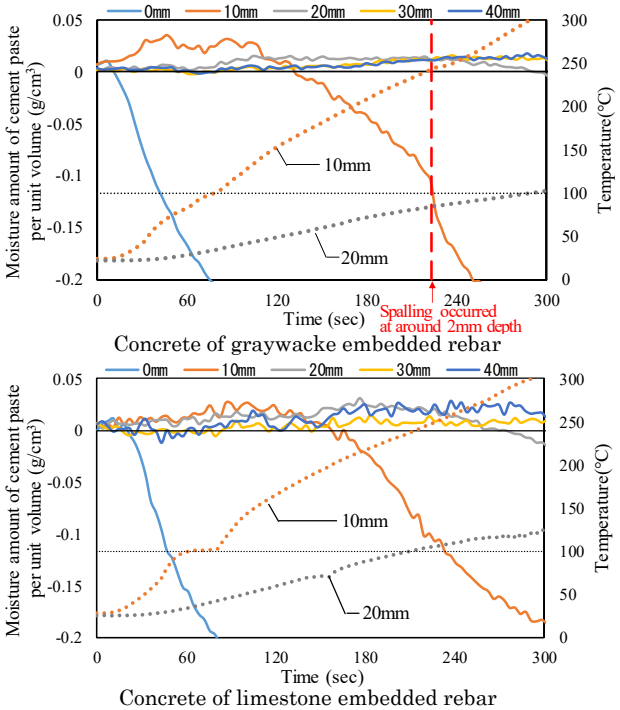

Fig. 3. Moisture and temperature profile evolution at different depths from the heating surface.

CO8-10 Development of capillary-plate-based flourescent plates for neutron radiography

T. Sakai[1], K. Kurita[1], H. Iikura[1], D. Ito[2], Y. Saito[2]

[1]*Materials Sciences Research Center, Japan Atomic Energy Agency*
[2] *Institute for Integrated Radiation and Nuclear Science, Kyoto University*

INTRODUCTION: Fluorescent plates are widely used for neutron radiography. In the case of the imaging devices, the spatial resolution of fluorescent plates conflicts with their detection efficiency. In general, a thicker phosphor layer increases the efficiency, but adversely affects the resolution because of blurring [1]. In this work, we developed a new approach to fabricate micro-structured fluorescent plates. The devices consist of capillary plates and fine phosphor grains [2]. Herein, we introduce the adding neutron sensitivity to the fine fluorescent plates for neutron imaging device.

EXPERIMENTS: The capillary plate is made from borosilicate glass. The specifications of the plates are as follows: plate thickness, 0.4 mm; diameter of each capillary, 25 μm; pitch of each hole, 31 μm; open area ratio, 59 %; diameter of effective area, 20 mm. The phosphor grains were sifted silver-activated zinc sulfide (ZnS:Ag) with a mean particle size of approximately 7 μm [1, 2]. The plates are impregnated with ^{10}B-enriched orthoboric acid to add neutron detection sensitivity. The method of impregnation is shown in Fig. 1.

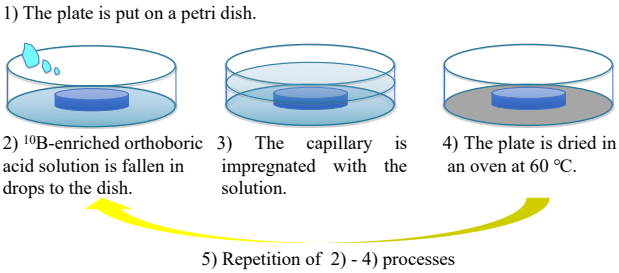

Fig. 1. Schematic of the orthoboric acidimpregnation method.

The neutron imaging experiments were performed at KUR E-2. The images were collected using a CCD camera, and the results are indicated in Fig. 2.

RESULTS: Neutron induced fluorescence is clearly observed, however the uniformity differs according to the drying time. Fig.2 (a) and (b) show that 1 hour drying times seems to be enough, but 20 minutes drying is not enough. The repetition times of impregnation increase neutron sensitivity as shown in Fig.2 (c) and (d).

We have developed the micro-structured fluorescent plates successfully. Impregnation with ^{10}B-enriched orthoboric acid is effective to add neutron sensitivity to the fluorescent plates. The fabricated fluorescent plates are expected to be useful in high-spatial-resolution imaging devices with good detection efficiency. The next step of the work is to increase the neutron detection efficiency. The metal coating inside the capillary walls is considered to be a promising method.

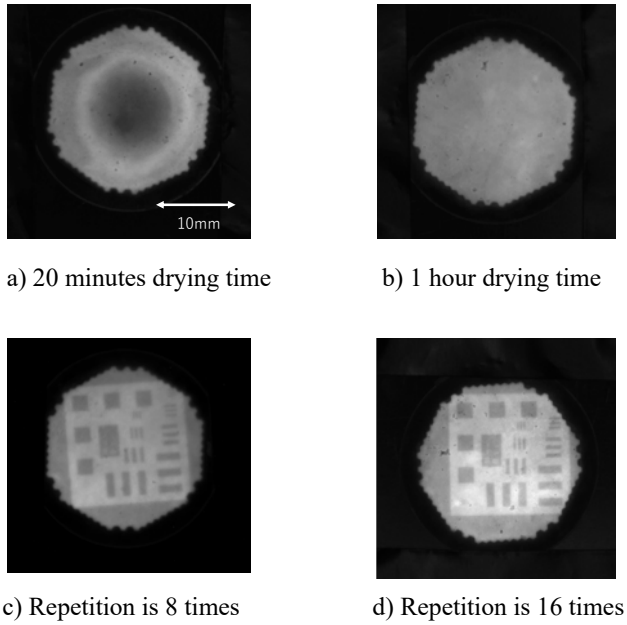

a) 20 minutes drying time

b) 1 hour drying time

c) Repetition is 8 times

d) Repetition is 16 times

Fig. 2. Results of fluorescent plates neutron imaging. Each plate was exposed to neutrons for 10 minutes. Image (a) drying time is 20 minutes, (b) drying time is 1 hour, respectively. Image (c) repetition of orthoboric acid lution is 8 times, (d) repetition is 16 times, respectively. In (c) and (d), the object is a line-pair indicator [3] .

REFERENCES:

[1] T. Sakai *et al.,* Nucl. Instr. and Meth. Phys. Res. B 332 (2014) 1238.
[2] T. Sakai *et al.,* JPS Conf. Proc. 11, 020005 (2016) .
[3] R. Yasuda *et al.,* Physics Procedia 43 (2013) pp.196-204.

CO8-11 Visualization of a Microchannel Heat Exchanger under Non-uniformly Heated Condition

H. Sakai, H. Umekawa[1], T. Ami[1], Y. Saito[2] and D. Ito[2]

Graduate School of Science and Engineering, Kansai University
[1]Department of Mechanical Engineering, Kansai University
[2]Institute for Integrated radiation and Nuclear Science, Kyoto University

INTRODUCTION: Recently, microchannel heat exchangers have been widely adopted in air-conditioning units, instead of conventional fin-tube heat exchangers which composed of copper tubes and aluminum fins. Microchannel heat exchangers have a lot of advantages, i.e. large specific surface area increases the heat-transfer performance, the small diameter reduces the amount of refrigerant and prevents the flow separation, and aluminum body reduces the weight and contact thermal resistance with aluminum fin. However, microchannel heat exchangers are consisted from many parallel mini channels, thus the control of flowrate in each channel is quite difficult. Especially as the heat exchangers for air-conditioning unit, the flow path of refrigerant is normal to the path of air flow, thus the heat flux distribution becomes non-uniform. Under these heating conditions, the flow maldistribution and flow instability in parallel channels may occur, and it reduce the performance of heat exchangers.

Several papers have been reported on heat transfer performance of microchannel heat exchangers so far. However, those investigations mostly treated the micro channel heat exchanger as one equipment, and the report treated the flow condition in each channels has been quite limited.

The main purpose of this investigation is understanding the heat and flow characteristics in each micro channel. In this report visualization results of a microchannel heat exchanger under non-uniform heating by using neutron radiography are briefly introduced.

EXPERIMENTS: Experiments of the visualization were carried out using the B-4 beam line in KUR (1 MW). The experimental apparatus is shown in Fig.1. The working fluid used in this study is Methanol (99.5% purity), which has low viscosity similar with actual refrigerant (R32) and enough attenuation coefficient for visualization. The experimental apparatus is consisted of a reserve tank, pump, test section. Test section is an actual aluminum microchannel heat exchanger of air-conditioning unit, and it is heated by joule heating by using two nichrome foils attached to the plate surface with electrical insulation of Kapton film. These nichrome foil heaters can be heated separately and which can achieve the non-uniform heating condition.

RESULTS: Fig. 2 shows the visualization results of microchannel heat exchange under heating condition. These figures are results under same total heat input with different heat flux ratio in two film heaters. The left side of each figure corresponds to the lower heat flux side, and the maldistribution of flow is clearly observed as the difference of void fraction distribution. On the basis on these results the influence of the heat flux ratio on the void fraction distribution will be qualitatively estimated. Moreover, by using the dynamic image the stability of flow condition may be reported in future.

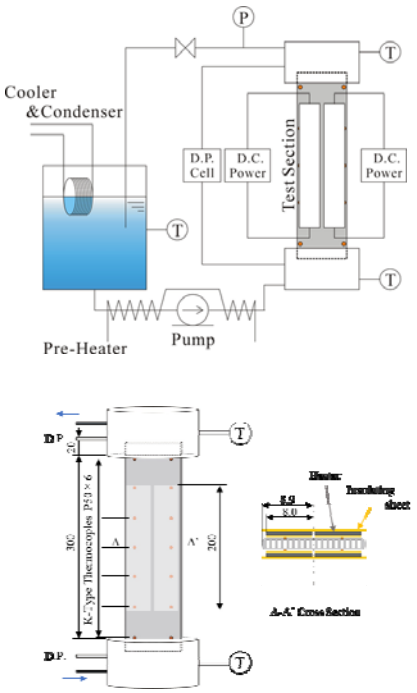

Fig. 1. Experimental apparatus.

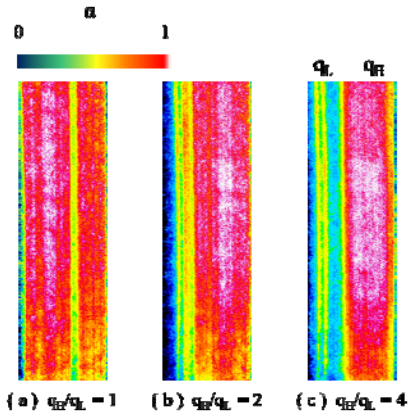

Fig. 2. Void fraction distribution.
($q_{average}$ = 40 kW/m^2, G = 150 kg/m^{2}s)

CO8-12 Diffusion Measurements on NASICON-Type Structured Lithium Ion Conductors by Means of Neutron Radiography

S. Takai[1], F. Song[1], H. Chen[1], K. Ota[1], T. Yamamoto[1], T. Yabutsuka[1], T. Yao[2], D.Ito[3] and Y. Saito[3]

[1]*Graduate School of Energy Science, Kyoto University*
[2]*Kyoto University*
[3]*Institute for Integrated Radiation and Nuclear Science, Kyoto University*

INTRODUCTION: Heterogenous doping effect, originally observed in halide solid state electrolytes, is proven to be favourable in oxide solid-state electrolytes by Onishi *et. al* [1]. Heterogenous doping is to disperse insulative particles in Li^+ ion conductors and create space charge layers at the vicinity of the insulative particles, which eventually improves the overall ionic conductivity of solid-state electrolyte [2]. Such dispersion system is referred as composite solid-state electrolytes.
In this work, neutron radiography method is applied to study the diffusion characteristics of LATP-4wt% LLTO composite solid-state electrolyte. Such technique has been a standardised method developed by our group, which utilises the difference in cross-section between ^7Li and ^6Li in neutron beam, such that the diffusion profile of $^6Li^+$ in ^7Li solid-state electrolytes can be visualised. This method eventually allows calculation of diffusion coefficient D^* of $^6Li^+$ [3-6].

EXPERIMENTS: Precursor of $^7Li_{1.3}Al_{0.3}Ti_{1.7}(PO_4)_3$ and $^7Li_{0.348}La_{0.55}TiO_3$ are synthesised by solid-state reaction method. By mixing the components in ratio of 96:4 and sintering, cubic pellets of ^7Li LATP-LLTO composite are prepared. $^6LiNO_3$ paste is applied to single side of the pellets, after which the pellets are annealed at different temperatures (300 °C, 400 °C and 500 °C) for 150 minutes to facilitate diffusion of ^6Li in ^7Li electrolytes. After cooling to room temperature, the pellets are subjected to direct neutron beam radiation at B4-port in KUR. The transmission neutron is converted to light signal by a converter plate, which is captured by a CCD camera.

RESULTS: The original radiography image and the intensity profiles are shown in Fig. 1. By Beer-Lambert's Law, the natural logarithm of I_N over I_0 is proportional to c_N, where I_N and I_0 are intensities of transmitted radiation with and without scattering, c_N is the light-scattering particle (in this case, $^6Li^+$). This allows conversion of intensity profiles into diffusion profiles which are shown in Fig. 2. It is assumed that $^6Li^+$ diffuses down the concentration gradient, and diffusivity of $^6Li^+$ is indifferent to its concentration. By the semi-finite solution to the Fick's equation, the diffusivities of $^6Li^+$ at different temperatures can be calculated, which are also shown in Fig. 2. It is evident that after annealing at 500 °C for 150 minutes, the $^6Li^+$ is homogenised across the entire ^7Li composite solid-state electrolyte.

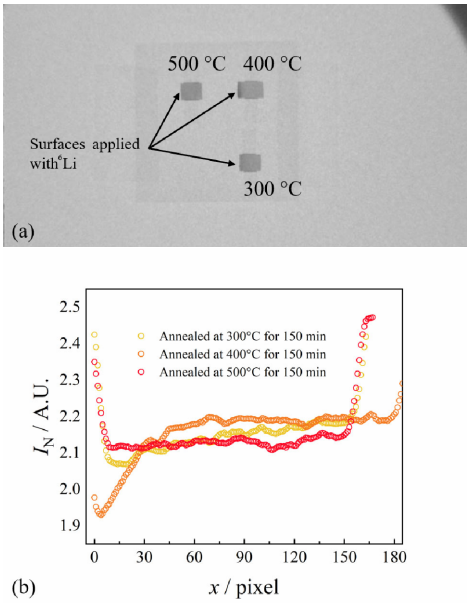

Fig. 1. (a) Original CCD camera photograph (radiography image) and (b) intensity profiles obtained by Image J.

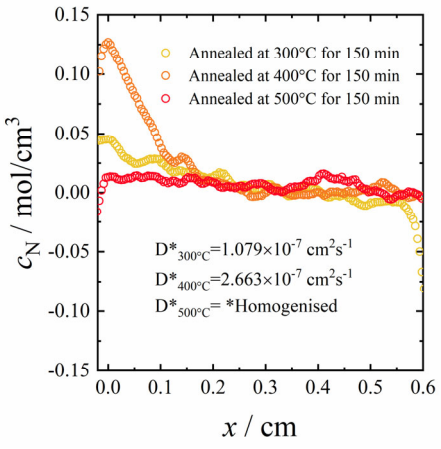

Fig. 2. Diffusion profiles and calculated diffusivity of $^6Li^+$.

REFERENCES:

[1] H. Onishi *et al*., *Electrochemistry*. **84** (2016) 967.
[2] C. C Liang. *J. Electrochemical Soc*., **120** (1973) 1289.
[3] S. Takai *et al*., *Solid State Ionics.*, **256** (2014) 93.
[4] S. Takai *et al*., *Solid State Ionics.*, **176** (2005) 2227.
[5] S. Takai *et al*., *Solid State Ionics.*, **171** (2004) 107.
[6] S. Takai, *et al*., *Solid State Ionics.*, **123** (1999) 165.

CO8-13 Study on the non-destructive nuclide assay for nuclear materials with a self-indication method

J. Hori[1], T. Sano[2], Y. Takahashi[1], and H. Yashima[1]

[1]*Institute for Integrated Radiation and Nuclear Science, Kyoto University*
[2]*Atomic Energy Research Institute, Kindai University*

INTRODUCTION: For decommissioning of Fukushima Daiichi Nuclear Power Plants, the identification and quantification of the nuclear material in fuel debris are important issues for appropriate nuclear material management. However, it is considered that fuel debris contains unknown amounts of minor actinides, fission products and neutron absorbers except for nuclear materials. Therefore, it is difficult to apply a conventional non-destructive assay to fuel debris. Neutron Resonance Densitometry (NRD) is one of the candidate techniques of non-destructive nuclide assay applicable to quantity nuclear materials in fuel debris. Especially, a self-indication method [1] is considered as a suitable technique for the identification and quantification of nuclides in fuel debris.

In the self-indication method, an indicator consisting of the target nuclide is placed at the neutron beam downstream from a sample. The self-indicator is a transmission neuron detector that has high efficiency around the objective neutron resonance energies of the target nuclide, enabling us to quantify effectively the amount of resonance absorption of the target nuclide.

In this study, we considered the possibility of nuclear discrimination imaging using a stationary neutron source as an application of the self-indication method. By inserting the self-indicator filter into the beam line, the transmitted neutrons around the objective neutron resonance energies are decreased especially. Therefore, we expect to identify the neutron absorption due to the target nuclide resonance without using a time-of-flight (TOF) information.

EXPERIMENTS: The experiment was performed at the 46-MeV electron linear accelerator in Institute for Integral Radiation and Nuclear Science, Kyoto University. The linac was operated with a repetition rate of 50 Hz, a pulse width of 4 μs, a peak current of about 0.5 A, and an electron energy of about 30 MeV. The pulsed neutron beam was collimated to 50 mm in diameter. Three foils of In, Ag and Ta were placed in the center of beam line at a distance of 12 m from the neutron source as shown in Fig. 1. A GEM detector (THIN-GEM, Bee Beans Technologies Co., Ltd.) was used as a neutron position sensitive detector. The detector can obtain the two-dimensional information of TOF for transmitted neutrons. A Cd sheet of 0.5 mm in thickness was inserted into the TOF neutron beam line to shield thermal neutrons. Runs with and without the sample (sample run and blank run) were carried out. Moreover, we performed the measurement with the sample and additional In filter of 0.5 mm in thickness as a self-indicator (sample with filter run).Each measurement time was about 10 hours.

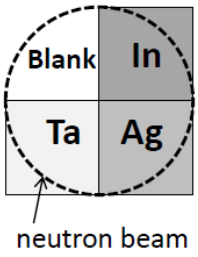

Fig.1 Sample arrangement of In, Ag, Ta foils for the present neutron imaging experiment.

RESULTS: Figure 2 shows the transmission neutron radiographs of the test sample illustrated in Fig. 1. The spatial distribution of the transmitted neutron flux was obtained by gating on the TOF region corresponding to the 1.46-eV resonance of In. The region of In was clearly identified as shown in Fig. 2(a). On the other hands, the spatial distribution of the relative counting rate in the sample with filter run to that in the sample run was obtained as shown in Fig. 2(b). Though the contrast between In and other materials was inferior to that of the imaging gated on the resonance, the region of In can be identified. It is noted that the radiograph was obtained without using TOF information. It indicated that the self-indication method can be utilized to the nuclear discrimination imaging using a stationary neutron source.

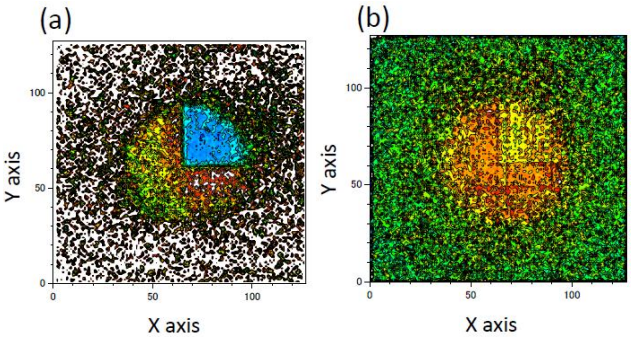

Fig.2 Neutron radiographs obtained by (a) gating on the resonance region of In and (b) using the relative counting rate in the sample with filter run to that in the sample run.

Present study was supported by JSPS KAKENHI Grand Number JP17K07012.

REFERENCES:

[1] J. Hori *et al.*, EPJ Web of Conferences, 146, 09042 (2017).

CO8-14 The measurability of photofission reaction of uranium induced by bremsstrahlung photons

K.W. Chin, H. Sagara, J. Hori[1], Y. Takahashi[1]

Tokyo Institute of Technology

[1]Institute for Integrated Radiation and Nuclear Science, Kyoto University

INTRODUCTION: Non-destructive assay technique for nuclear material is one of the most important technical issues in the field of safeguard. A non-destructive assay using photonuclear reaction has been considered as a promising one. Previous work suggested new method using a mono-energy Gaussian photon beam to measure the isotopic composition of nuclear fuel materials without relying on their self-generated neutron information [1]. However, producing a Gaussian photon beam requires costly laser Compton scattering instrument. Thus, this re-search aims to replace the source with a blemsstrahlung photon beam from an accelerator[2]. In this work, we tried to perform the feasibility study on the detection of prompt neutron produced by the photonuclear reaction in the ura-nium sample.

EXPERIMENTS: The experiment was performed at the KURNS-LINAC. A natural uranium sheet was used as a sample and placed in the center of beam line at a distance of about 12 m from the photon source. A platinum target was used as the photon source of bremsstrahlung. The linac was operated with a pulse repetition rate of 100 Hz. The energy of electron was optimized to 18 MeV based on the parameter survey in the range from 8 to 30 MeV. An organic liquid scintillator (BC-501A) with a high perfor-mance associated with the discrimination ability between neutron and gamma ray was used as a neutron detector. The detector was placed at a distance of 10 cm from the sample. The signals from the detector were taken in the pulse-shape discrimination system and the two-dimen-sional data of pulse height and rise time were obtained. We carried out six kinds of measurements. Three measure-ments were done with no sample and standard sources (Cf-252, Cs-137) without linac operation. The remaining measurements were done with linac operation in the fol-lowing conditions of no sample without shields, a natural uranium sample with a neutron shield, and a natural ura-nium sample with neutron and gamma-ray shields. In the linac experiment, intense gamma flush and photo-neutron from the target is obstructive to the measurement of prompt neutron from the sample. Therefore, two polyeth-ylene blocks and two lead blocks were used as shielding materials. Moreover, the electron beam current was re-duced from 91 μA to 2 μA to inhibit the effect of gamma flash for every run.

RESULTS: Two-dimensional data of pulse height and rise time were shown in Fig. 1 for six measurements, re-spectively. It is noted that the horizontal axis is rising time whereas the vertical axis is pulse height. At first, we can identify the region of interest (ROI is shown as the dotted box) as neutron events by comparing the run of Cf-252 with that of Cs-137. However, a few gamma-ray events were unfortunately observed in the ROI and those should be taken account of background. The counting rate for each run in the ROI is shown in Table 1. We observed a significant difference between the run of no sample and that of uranium sample with neutron and gamma-ray shields. Further analysis and experiment were necessary in order to obtain conclusive evidence of the measurability of neutron caused by photoreaction.

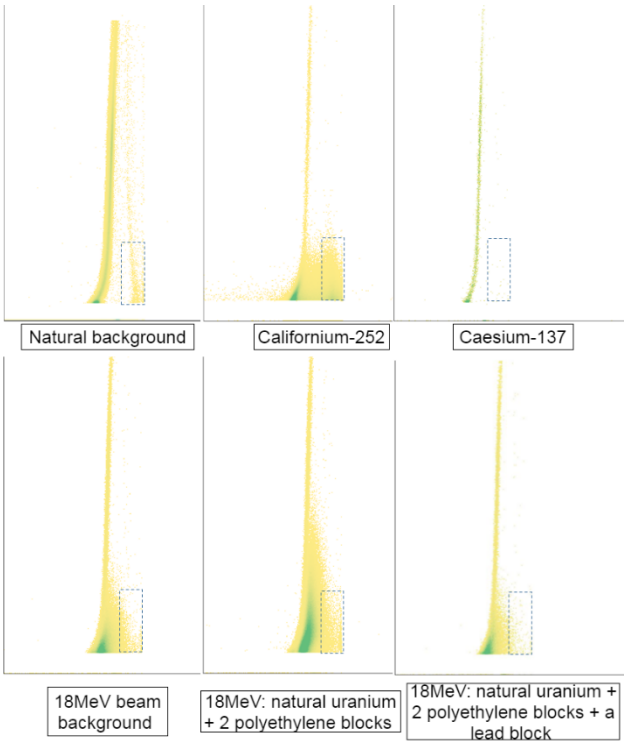

Fig. 1. Different cases of natural background, ^{252}Cf, ^{137}Cs, 18 MeV beam backg round and natural uranium.

Table 1. Statistical data of counting in ROI.

ROI Cases	Total count rate, cps	To-tal coun ts, N	Absolute error,	Relative error,
Natural BG	0.02158	1025	32.0	0.0312
$BG_{beam\text{-}18MeV}$	0.2094	754	27.5	0.0364
^{252}Cf	75.87	45706	213	0.0046
NU+PolyB	0.7754	2793	52.8	0.0189

REFERENCES:

[1] R. Kimura *et al.*, JNST, **53(12)**, (2017).
[2] K.W. Chin *et al.*, AESJ, Univ. Ibaraki, (2019).

CO8-15 Distribution of coolant inside a flat laminate vapor chamber in a vertical posture

K. Mizuta, Y. Saito [1] and D. Ito [1]

Faculty of Engineering, Kagoshima University
[1]Institute for Integrated Radiation and Nuclear Science, Kyoto University

INTRODUCTION: Recently, severity in the cooling electronic devices is increasing because of shrinking size of such devices. Poor ability of heat exhausting system leads to various problems such as low reliability and low working efficiency of semiconductor. Various types of vapor chambers are attracting attention than ever with a hope for solving such problems by higher heat spreading ability of vapor chambers. In the practical use of vapor chambers, postural effect on thermal performance of vapor chambers is very important, because the change in the thermal performance of vapor chamber with posture, if it occurs, may restrict the performance of the electronic devices. A flat laminate vapor chamber called FGHP (Fine Grid Heat Pipe) is one of the most promising candidates to solve such thermal problems, with the highest heat spreading ability concerning the overall heat transfer coefficient based on the area of heat source [1]. Our pre-vious study shows that the effect of gravity on the coolant distribution of FGHP is negligible [2].

In this study, we investigated the gravitational effects on the coolant distribution in the FGHP by using neutron radiography at the Kyoto University Research Reactor (KUR) with higher input and smaller heat source than our previous work.

EXPERIMENTS: Experiment was conducted at the E-2 port of the KUR, where the thermal neutron flux at the sample position was about 3×10^5 cm^2s at 5 MW operation. The size of the test sample of FGHP heat spreader was 65 mm square and 2 mm thick. The test sample was set vertically, which means that its bottom and top plate was placed parallel to the gravitational direction. Figure 1 shows the experimental setup. A ceramic heater of 10×10 ×1.75 mm^3 was attached to the central part of the bottom plate as a heat source, and the top plate was cooled by plate-fin type aluminum heat sinks of 70×70 mm^2 under forced convection conditions. K-type ther-mocouples were utilized to measure both surface temper-ature of the heat spreader and the atmospheric tempera-ture to estimate the thermal resistance. A CCD camera (BU-53LN, BITRAN Co. Ltd.) was utilized, which has 4008×2672 pixels and ^{6}LiFZnS (50 μm thickness) was used as a scintillator screen. The spatial resolution was 9.0 μm/pixel at the present system setup, however, the effective spatial resolution was about 50 μm/pixel due to the scintillator screen characteristics. Neutron imaging of the sample was performed at the 1 MW operation mode of the KUR and the exposure time was 300 s. Neutron images of the sample were utilized to calculate liquid thickness in the FGHP. The effect of gravity on the coolant distribution was evaluated by the calculated liquid thickness in the wick area at different four positions.

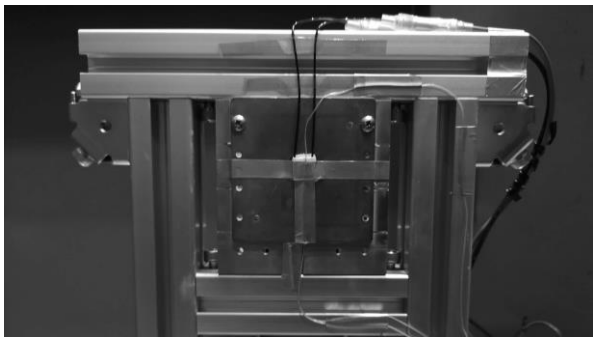

Fig. 1 Experimental setup.

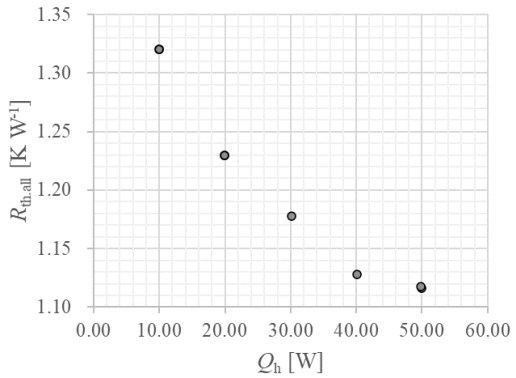

Fig. 2 Variation of total thermal resistance of the system with heat input (Q_h).

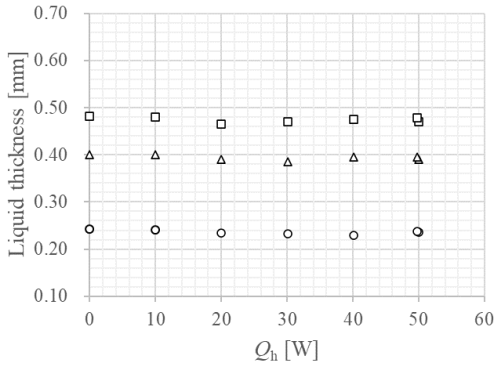

Fig. 3 Variation of liquid thickness with heat input. (○:top, □:bottom, △:horizontal average)

RESULTS: Figure 2 shows the variation of total thermal resistance of the system with heat input (Q_h). As shown in Fig. 2, thermal resistance decreased with increasing heat input, as reported in the previous work [1]. Figure 3 shows that liquid thickness at various positions were almost constant regardless of heat input, which means that FGHP work properly with about 20 times higher heat flux than the previous work [2].

REFERENCES:

[1] Mizuta, K., *et al.,* Applied thermal management, **104** (2016) 461-471.
[2] Mizuta, K., *el al.*, Physics Procedia, **69** (2015) 556-563.

CO8-16 Demonstration experiments of an innovative method to detect nuclear material

M. Komeda, Y. Toh, Y. Kitamura[1], T. Misawa[1] and K. Tanabe[2]

Nuclear Science and Engineering Center, Japan Atomic Energy Agency

[1]Institute for Integrated Radiation and Nuclear Science, Kyoto University

[2]National Research Institute of Police Science

INTRODUCTION: A compact and low-cost non-destructive assay system to detect hidden nuclear material is required in the fields of nuclear security. We have therefore developed an innovative nuclear material detection method by using a neutron source of Califor-nium-252, which is capable to assemble such system [1]. In this method, a neutron source is rotated at a speed of thousands of rpm nearby the target. Meanwhile, it is pos-sible to detect nuclear materials by confirming the de-formation of the time-distribution spectrum obtained by a neutron detector near the target. The machine to rotate the neutron source is less than 60 cm in width, depth, and height. The rated output of the motor is only 750W. We installed the machine at an experimental laboratory in the KUCA, and carried out demonstration experiments using a neutron source (5MBq of Cf-252) and uranium.

EXPERIMENTS: Figure 1 shows the overview of apparatuses used in the experiment. A neutron source was installed at the outer periphery of a disc of 32 cm diameter. The uranium sample that was surrounded with polyethylene moderator set between the rotation machine and neutron detectors. The neutron detector system consists of 6 He-3 proportional counters, which are wrapped with a cadmium plate and a boron rubber sheet in order to detect only fission neutrons effectively. The time distribution of neutron measurement was performed by a multi-channel scaler (MCS) that is synchronized with the disc rotation. A measurement time was 15 minutes for each experiment.

RESULTS: Figure 2 shows an example of experimental results of a natural uranium sample and a blank sample under the condition that the rotation speed is 4000 rpm. The polyethylene moderator was utilized in the meas-urements of both the uranium and blank samples. The neutron source was closest to the uranium sample ap-proximately at 6300 micro-seconds in Figure 2. Since the neutron source, the uranium sample, the polyethylene moderator and the neutron detector system have a com-plicated geometry, the dips appear before and after the peak. When the uranium sample was used, data after 6300 micro-seconds (from 6300 to approximately 9000 micro-seconds) had higher counts compared to the blank sample. This is due to the delay effect of the interrogation neutrons (Cf-252 neutrons). The delay effect can be ob-served only when a sample contains a fissile material under a condition of high speed rotation of Cf-252. We could detect nuclear material for the first time by using the present new method. Thus, we could verify the innovative nuclear material detection method through these experiments at KURNS. This study and experiment would make a large impact in the field of nuclear security. A further study would be required to confirm the effects in various conditions, such as positional dependence of nuclear material, and would be conducted in near future.

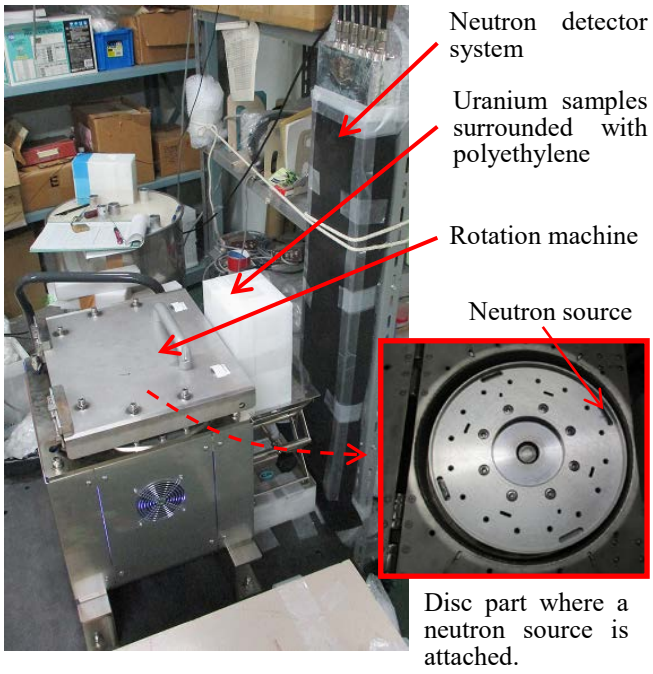

Fig. 1. Overview of experimental devices.

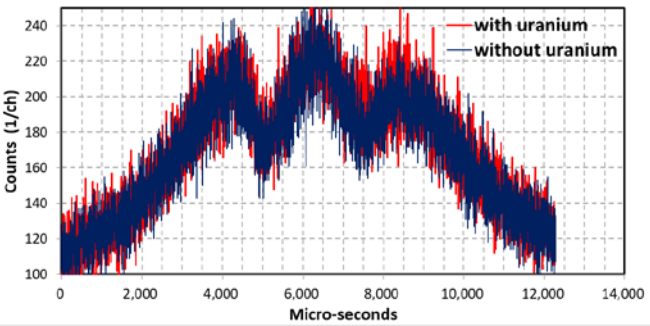

Fig. 2. Experimental examples of the uranium sample (red line) and blank sample (blue line). The measurement time was 15 minutes with the rotation speed of 4000 rpm.

REFERENCES:

[1] M. Komeda, Y. Toh, Annals of Nuclear Energy, **135 (2020)** 106993.